

Perovskite Light-Emitting Diodes



Dawei Di and Baodan Zhao

1 Introduction

Perovskite light-emitting diodes (PeLEDs) [1] are an emerging technology for next-generation display, lighting, and communications. They offer the combined advantages of excellent color purity, spectral tunability, high luminescence efficiencies, and low processing costs. Since the report of room-temperature electroluminescence (EL) from halide perovskite in 2014 [1], the field has been moving at an unprecedented pace; the external quantum efficiencies (EQEs) of PeLEDs exceeded the 20% milestone in 2018 [2–5], followed by more recent works improving the device EQEs to ~28% [6].

Advances in material development and device structures were the main driving forces for the rapid progresses in device performance. The device designs of early PeLEDs were heavily inspired by that of perovskite solar cells and polymer OLEDs [1, 7, 8]. While PeLEDs are typically processed very simply from solution, they show optoelectronic characteristics comparable to that of conventional III–V devices, which require demanding processing conditions [9, 10]. Similar to other types of LEDs, enhancing the radiative recombination processes while reducing the nonradiative recombination losses holds the key to raising the internal quantum efficiencies (IQEs) of PeLEDs toward 100% [3, 10]. To achieve this goal, the emissive layer materials were improved primarily by compositional engineering and dimensionality control [3, 11, 12].

Innovations in device architectures were critical to the realization of the current state-of-the-art devices [2–6, 13, 14]. For PeLEDs with different colors, device

D. Di (✉) · B. Zhao (✉)

State Key Laboratory of Extreme Photonics and Instrumentation, College of Optical Science and Engineering; International Research Center for Advanced Photonics, Zhejiang University, Hangzhou, China

e-mail: daweidi@zju.edu.cn; baodanzhao@zju.edu.cn

designs vary considerably due to the different scenarios of charge injection, blocking, and balance. It has been understood that reducing nonradiative recombination losses at the emissive layer/charge-transporter interfaces [3, 13, 15] of PeLEDs is equally crucial, if not more crucial than suppressing nonradiative recombination in the bulk region. While the IQEs of PeLEDs were found to approach unity [3], the EQEs are restricted by the relatively poor light extraction efficiency of the device architecture [3, 16, 17]. This indicates opportunities in improving device efficiency through light management.

While great progresses have been made in improving PeLEDs to become a commercially viable technology, many challenges remain. The poor device operational lifetimes are considered the main obstacle toward industrial applications. A recent breakthrough in this direction was the demonstration of ultrastable near-infrared (NIR) PeLEDs with device lifetimes meeting the demands of commercial applications [18]. However, the operational stability of visible PeLEDs remains poor. Among various stability-limiting mechanisms, ion migration and phase instability are some of the most crucial factors for the instability of PeLEDs. Besides, high-performance blue [19, 20] and white [21, 22] PeLEDs are still under active development, and they are important missing pieces for perovskite-based full-color display and solid-state lighting applications. Moreover, issues concerning the toxicity of lead [23, 24] and the progress in the development of mini- and micro-PeLEDs [25] require attention from researchers in the field.

2 Device Architectures

The commonly used device structures for PeLEDs were mostly inherited from that of planar perovskite solar cells and solution-processed OLEDs [1, 7, 8]. The perovskite emissive layer is normally placed in between charge-transport layers (CTLs) with different polarities (e.g., electron- and hole-transport layers) to form a sandwich-like device structure [1]. One of the CTLs is normally in contact with a conductive oxide-coated transparent substrate, while the other CTL is in contact with metal electrodes.

The CTLs are normally considered to serve two functions simultaneously: charge transport and charge injection into the perovskite emissive layers. Using terminologies borrowed from conventional semiconductor diodes, the current PeLED structures may be comparable to that of a PIN heterostructure LED. In direct reference to thin-film OLEDs, a “standard” device configuration refers to the structure in which the hole-transport layer (HTL) such as PEDOT:PSS is in contact with the transparent conductive substrate, while the electron-transport layer (ETL) such as TPBi is coated by thermally evaporated electrodes (e.g., LiF and Al) (Fig. 1a) [1, 13, 14]. An “inverted” device structure normally refers to the case where the ETL such as ZnO is deposited on top of the transparent conductive substrate and the HTL such as TFB polymer is coated by thermally evaporated electrodes (e.g., MoO_x and Au) (Fig. 1b) [12, 27].

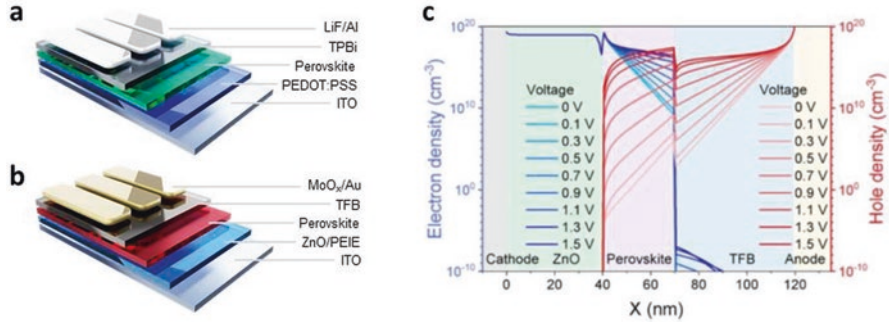


Fig. 1 Device structures and charge distribution of typical PeLEDs. Schematic illustrations of (a) the structure of a typical PeLED with a “standard” configuration and (b) the structure of a typical PeLED with an “inverted” configuration. (c) Simulated electron and hole density distributions in the perovskite LED under different voltages. The shaded regions in gray, light green, pink, light blue, and yellow correspond to cathode, ZnO, perovskite, TFB, and anode, respectively. Panels **a** and **b** were reproduced from [18]. Panel **c** was reproduced from [26]

3 General Device Operation

The basic operation principles of PeLEDs are similar to that of inorganic semiconductor heterojunction LEDs, with some deviations in charge injection and transport due to the commonly used device configurations in which organic CTLs are employed.

3.1 Charge Injection and Blocking

When an external bias is applied to a PeLED, charge injection from the electrodes to the CTLs occurs by drift and diffusion processes, followed by the subsequent injection of charges into the perovskite emissive layer. The simplest consideration for efficient charge injection is the correct alignment of energy levels between the neighboring materials in the PeLED structure. For example, the LUMO level of the ETL is normally close to the conduction band minimum (CB) of the perovskite emissive layer to ensure effective electron injection. At the same time, the ETL prevents excess hole current from passing through the device. This is normally ensured by the deep-lying HOMO level of the ETL. The distribution of charges across a typical PeLED is shown in Fig. 1c [26].

It should be noted that closely aligned energy levels are not strictly required for efficient charge injection in cases where the CTLs are highly conductive. For example, the valance band maximum (VBM) of ITO is around 4.5 eV, showing a considerable energy-level offset of ~0.6 eV with the commonly used PEDOT:PSS HTL (HOMO: 5.1 eV). ITO/PEDOT:PSS is known to be an excellent hole-transport interface for PeLEDs despite the large energetic offset. This could be understood by the high carrier concentrations and mobilities in both the ITO and PEDOT:PSS

materials, allowing the formation of ohmic contact at the interface without the need of closely aligned energy levels. The blocking of charges by CTLs of the opposite polarities prevents leakage currents, raising the chance of electron-hole encounter.

3.2 Charge Recombination

The recombination of carriers in halide perovskite materials shows many similarities to that of inorganic semiconductors such as III–V compounds [9, 10]. Excited-state carriers in typical three-dimensional (3D) halide perovskites are in the form of free carriers or loosely bound electron-hole pairs due to the large dielectric constants that screen Coulomb interactions, showing exciton binding energies on the order of 10 meV [28]. The optically or electrically injected carriers in the perovskite material relax radiatively through band-to-band recombination, giving rise to light emission.

In addition to the radiative recombination channel discussed above, there are non-radiative recombination losses that are responsible for the non-ideal light emission efficiencies of the perovskite materials and devices. Trap-assisted (Shockley-Read-Hall) recombination is the main mechanism for nonradiative losses at moderate to low carrier densities. For MAPbI₃ perovskite, trap-assisted recombination is expected to dominate at carrier density of $<10^{16}$ cm⁻³ [29], which is relevant to solar cell and LED operation. Trap passivation is therefore a critical consideration in raising PeLED performance. Under higher carrier densities, Auger recombination [29, 30] is expected to occur, leading to efficiency losses at higher current densities.

Assuming balanced electron and hole populations in the perovskite emitter, the recombination of injected carriers can be described by the following equation:

$$-\frac{dn}{dt} = k_1 n + k_2 n^2 + k_3 n^3 \quad (1)$$

where k_1 is the trap-assisted recombination rate, k_2 is the rate constant of band-to-band radiative recombination, k_3 is the Auger recombination constant, and n is the carrier concentration [28].

Assuming only band-to-band recombination contributes to the radiative process, the radiative efficiency η_{rad} is therefore given by Eq. (2) and is used to describe the power dependent PLQEs observed for typical perovskite emitters (Fig. 2a):

$$\eta_{\text{rad}} = k_2 n / (k_1 + k_2 n + k_3 n^2) \quad (2)$$

It has been suggested that in low-dimensional perovskite emitters with lower dielectric constants, excited-state carriers may exist in the form of excitons which may recombine radiatively in a fashion more similar to that in organic semiconductors [31, 32]. This could make the first-order term ($k_1 n$) of Eq. (1) completely or partly radiative, raising the radiative efficiency at medium to low carrier densities.

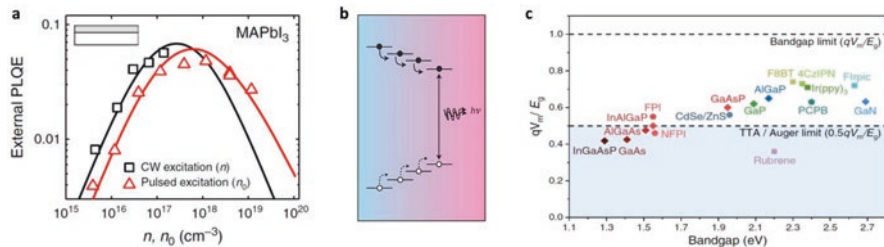


Fig. 2 Studies of radiative recombination for PeLEDs and related devices. **(a)** Measured external PLQEs for MAPbI₃ perovskite under steady state (black) and pulsed laser excitation (red) with the prediction from the recombination rate model (lines). Under pulsed excitation, the average PLQE is measured over the decay of the carrier density n . **(b)** Multi-phase perovskite material $\text{PEA}_2(\text{CH}_3\text{NH}_3)_{n-1}\text{Pb}_n\text{I}_{3n+1}$ channel energy across an inhomogeneous energy landscape, concentrating carriers to the smallest-bandgap emitters. The arrows represent the carrier transfer process. **(c)** Measured qV_m/E_g of different classes of LEDs. FPI, NFPI, and PCBP denote FAPbI_3 , $\text{NMA}_2\text{FA}_{n-1}\text{Pb}_n\text{I}_{3n+1}$, and $\text{PEA}_2\text{CS}_{n-1}\text{Pb}_n\text{Br}_{3n+1}$ perovskite, respectively. The shaded area denotes the region where the measured qV_m/E_g falls below the limits set by TTA or Auger processes. Panel **a** was reproduced from [29]. Panel **b** was reproduced from [11, 12]. Panel **c** was reproduced from [26]

3.3 Energy Transfer/Funneling

A distinct branch in PeLED research is the study of mixed-dimensional perovskite systems exhibiting efficient energy transfer/funneling from the higher-bandgap to the lower-bandgap perovskite phases. This mechanism confines charges at the lower-bandgap perovskite crystal domains, enabling interfacial passivation and an increased local carrier concentration that enhance radiative recombination processes (e.g., a larger k_2n^2 term in Eq. (1)).

Such mechanism was found to be effective in PeLEDs operating at moderate current densities. However, due to the high local carrier concentrations, Auger recombination in mixed-dimensional perovskite emitters were found to be more pronounced [33], contributing to efficiency roll-off at higher current densities.

3.4 Operating Voltages

Recently, it was reported that the minimum voltage required for observing EL from PeLEDs could be as low as $0.46E_g/q$, where E_g is the bandgap and q is the elementary charge [26]. Ultralow operating voltages were universally observed across many classes of semiconductors (Fig. 2b) [26], in contrast to earlier reports claiming up-conversion mechanisms exclusive to a few material systems. The ultralow-voltage EL phenomenon does not violate the energy conservation principle and can be explained by the recombination of band-edge carriers whose populations are determined by Fermi-Dirac functions perturbed by a small external bias. However, the apparent threshold voltages for a particular photon flux vary greatly for different classes of LEDs [26].

For example, a unique benefit of PeLEDs over OLEDs is that they generally operate at lower driving voltages for the same photon flux. This is primarily due to the reason that metal halide perovskites exhibit higher carrier concentrations and mobilities at room temperature compared to organic semiconductors. It was shown that PeLEDs can be driven at voltages below the bandgap of silicon, allowing potential integration with silicon electronics [26]. The low operating voltages of PeLEDs indicate opportunities in next-generation communications, computational and energy applications.

4 Achieving Near-Unity Internal Quantum Efficiencies

A critical step in establishing PeLED as a next-generation light source technology was the demonstration of high EL quantum efficiencies [2–6, 15]. The EQE and IQE of PeLEDs are correlated with each other according to the following equation:

$$EQE = IQE \times f_{\text{outcoupling}} = f_{\text{balance}} \times f_{\text{e-h}} \times \eta_{\text{rad}} \times f_{\text{outcoupling}} \quad (3)$$

where f_{balance} is the charge injection balance factor (with a maximum value of unity), $f_{\text{e-h}}$ is the probability of forming a correlated electron-hole pair from each pair of injected carriers, η_{rad} is the probability of radiative recombination for each electron-hole pair, and $f_{\text{outcoupling}}$ is the optical outcoupling coefficient [28].

It can be seen that IQE is determined by f_{balance} , $f_{\text{e-h}}$, and η_{rad} . Charge balance (f_{balance}) can be maximized by choosing functional layers with appropriate energy levels [3, 4, 34, 35] and charge-transport properties [13]. The main strategies for improving $f_{\text{e-h}}$ include the formation of charge-confinement structures that improve the chance of electron-hole encounters [11, 12, 35] and the enhancement of Coulomb interactions by reducing the dielectric constants of the materials [28, 33]. For perovskite emitters, the radiative efficiency of an electron-hole pair (η_{rad}) is determined by $\eta_{\text{radiative}} = k_{\text{rad}} / (k_{\text{rad}} + k_{\text{non-rad}})$, where k_{rad} is radiative recombination rate and $k_{\text{non-rad}}$ is the nonradiative recombination rate [28]. For emitters where only band-to-band recombination contributes to photon emission, η_{rad} can be obtained by Eq. (2) discussed earlier.

4.1 Suppressing Bulk Nonradiative Losses

The most intensively studied direction in the field of PeLEDs has been the suppression of nonradiative losses in the bulk region of the perovskite emissive layer. The suppression of nonradiative losses ties closely with the passivation of traps in the perovskite materials. This was typically achieved by compositional tuning of the perovskite precursors [14, 27], introduction of small molecule [36] and polymeric [3] trap passivators, dimensionality control [11, 12], and post-treatments [14, 20].

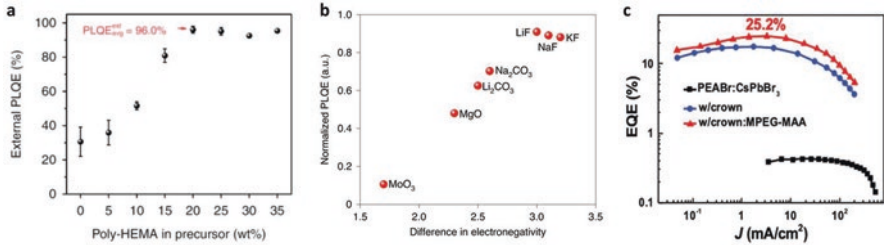


Fig. 3 Suppressing nonradiative losses for PeLED materials and devices. **(a)** External PLQE of perovskite-polymer bulk heterostructure films (on fused silica) as a function of poly-HEMA weight fraction in the solid precursors. The error bars show the highest and lowest external PLQEs measured for each weight fraction. The black dots represent the average external PLQEs. The optimized polymer weight fraction of 20% in precursor corresponds to a volume fraction of 28% in the emissive film. The excitation source used was a 532-nm c.w. laser with an intensity of 100 mW cm^{-2} (approximately 1 sun). **(b)** Normalized PLQEs of perovskite films formed on a range of thermally evaporated interfacial materials with different polarities, characterized by the relative electronegativity of the chemical bonds. **(c)** EQE– J characteristics of PeLEDs based on PEABr:CsPbBr₃ perovskite with/without crown and with crown:MPEG-MAA. Panel **a** was reproduced from [3]. Panel **b** was reproduced from [13]. Panel **c** was reproduced from [6]

Photoluminescence quantum efficiencies (PLQEs) of perovskite emissive layers are an indication of the effectiveness of passivation. PLQEs of approaching 100% were reported for perovskite-polymer heterostructures (Fig. 3a) [3] and perovskite nanocrystals [5]. Deep-lying traps responsible for the loss of PLQEs were considered to primarily originate from uncoordinated lead (including Pb²⁺ and Pb⁰) for the case of lead halide perovskite emitters. Other widely employed approaches for studying nonradiative losses are the characterization of trap density using space-charge limited current (SCLC) analysis [23] and the measurements of PL decay kinetics which are affected by the rates of both radiative and nonradiative recombination processes. The aforementioned methods are powerful tools in the development of perovskite emissive layers for PeLEDs.

4.2 Suppressing Interfacial Nonradiative Losses

Interfacial nonradiative recombination is a critical factor limiting the performance of PeLEDs. However, this issue did not receive as much attention as for the losses in the bulk. An example of interfacial nonradiative losses in PeLEDs is the reduction of PL lifetime and intensity (PLQE) when the emissive layer is in contact with the charge-transport layers [3]. Such processes prevent PeLEDs from achieving near-unity IQEs, despite the very high PLQEs of the perovskite emissive layers.

Interfacial nonradiative losses in PeLEDs can be suppressed in various ways. First, approaches that provide bulk passivation could normally lead to the passivation of interfacial traps at the same time. For example, perovskite-polymer bulk heterostructures were found to eliminate the effects of interfaces on PL decay

kinetics, leading to near-unity IQEs and EQEs of up to 20.1% [3]. It was reported that ultrathin polar interfaces including lithium fluoride (LiF) [13] (Fig. 3b) enable the formation of highly emissive and uniform perovskite films on hydrophobic polymeric charge transporters in an OLED-like device configuration. This led to the demonstration of efficient green quasi-2D PeLEDs with EQEs of up to 19.1% at $>1500 \text{ cd m}^{-2}$. Similar interfacial modification and polymer passivation approaches were employed in green PeLEDs (Fig. 3c) showing exceptionally high EQEs of up to 28.1% [6]. Similarly, hydrophilic interfaces prepared using polymers such as polyethyleneimine [27], perfluorinated ionomer (PFI) [14], and small molecules including ethanolamine [37] and aluminum oxide [38] were found to allow the formation of high-quality perovskite films. Although these strategies have been proven useful for high-performance PeLEDs, further mechanistic investigations are required to reveal the origins of such improvements.

5 Light Outcoupling

While the IQEs in some of the best-performing PeLEDs approach 100%, around 80% of the internally generated photons are trapped in the device stack and eventually lose energy through a variety of loss channels owing to the non-ideal light outcoupling [2–5, 15].

Low light outcoupling yields in PeLEDs normally arise from (i) waveguide modes parallel to the substrate due to the larger refractive indices of perovskites (~ 2.5) compared to the commonly used charge-transport materials and transparent electrodes ($\sim 1.7\text{--}1.8$) [3] and (ii) the total internal reflection of emitted photons over a wide range of emission angles owing to the difference between the refractive indices of the device substrate and the air. Consequently, only photons from a small emission cone can escape from the PeLED device (Fig. 3c), while the rest are trapped in waveguided and substrate modes.

Opportunities in improving EQEs further lie in the ability in extracting the trapped photons from PeLEDs. Light outcoupling strategies for PeLEDs can be briefly divided into two categories, modifications of the perovskite layer properties and the employment of external optical structures.

5.1 Modification of Perovskite Layer Properties

Some notable approaches for light outcoupling based on the modification of the perovskite layer properties are the reduction of refractive index (n) [3], control of transition dipole moment orientations [39–44], formation of light scattering structures within the emissive layer [2], and photon recycling [16]. According to the ray optics limit of $1/2n^2$, the reduction of n can increase η_{out} for planar PeLEDs. For typical 3D perovskites, n is ~ 2.5 . Including 2D ligands with a significant fraction of

organic content in the perovskite composition lowers n to ~ 2.1 [3]. Introducing polymers into the perovskite emissive layers was reported to reduce n further to ~ 1.9 [3], resulting in an η_{out} of $\sim 21\%$ (Fig. 4a) and EQEs of up to 20.1% [3]. Orientation of transition dipole moments (TDMs) also plays an important role in the photon extraction processes. Emission from only horizontally oriented TDMs can be effectively extracted. The fraction of horizontal TDMs could be tuned by engineering the perovskite nanostructures [39–42, 44]. For PeLEDs based on nanoplatelets [39], a horizontal dipole fraction of $\sim 84\%$ and η_{out} of 31% were reported. Tuning of the fraction of horizontal TDMs can also be achieved for solution-processed polycrystalline perovskite films [43]. Light scattering in rough or structured emissive layers is expected to enhance η_{out} . PeLEDs based on submicrometer-scale structures were reported to have outcoupling efficiencies of $\sim 30\%$, leading to peak EQEs of up to 20.7% (Fig. 4b) [2].

Photon recycling improves the light extraction from PeLEDs by randomizing the directions of trapped photons in a fashion similar to scattering, but through the reabsorption and re-emission of light (Fig. 4c) [16, 28, 29, 45]. It was reported that for PeLEDs based on perovskite emitters with high internal radiative efficiencies and small Stokes shifts (e.g., $\text{PEA}_2\text{Cs}_{n-1}\text{Pb}_n\text{Br}_{3n+1}$), about 30–70% of EL may originate from photon recycling [16]. The theoretical outcoupling efficiency of PeLEDs in the presence of photon recycling is given by

$$EQE_{PR} = f_{\text{balance}} \times f_{\text{out,direct}} / \left[f_{\text{out,direct}} + A_{\text{para}} + \frac{(1 - \eta_{\text{rad}})}{\eta_{\text{rad}}} \right] \quad (4)$$

where f_{balance} is the charge balance factor, $f_{\text{out,direct}}$ is the direct light outcoupling efficiency, η_{rad} is the internal radiative efficiency of the perovskite layer, and A_{para} is the parasitic absorption loss external to the perovskite layer [16].

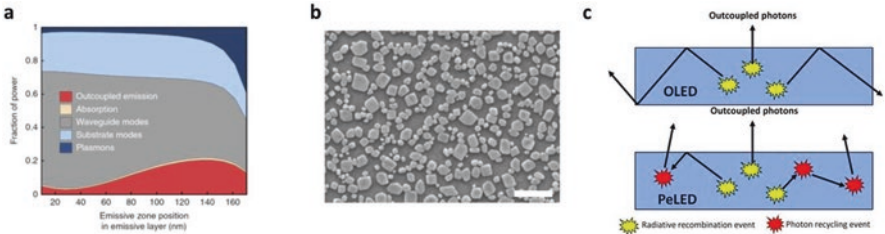


Fig. 4 Case studies of light outcoupling in PeLEDs. (a) Modeled fractional optical power distribution in the LED structure as a function of emissive zone position in the PPBH emissive layer with a thickness of 180 nm. The origin of the x-axis is the ETL/emissive layer interface. “Outcoupled emission” indicates the fraction of outcoupled light from the LED. Other modes lead to optical losses. (b) SEM image of the perovskite with submicrometer-scale structures. The scale bar represents 1 μm . (c) Simplified schematics for comparing light outcoupling processes in an OLED (upper panel) and PeLED (lower panel), with the arrows denoting photon trajectories. Panel a was reproduced from [3]. Panel b was reproduced from [2]. Panel c was reproduced from [28]

5.2 External Optical Structures

External optical structures such as lenses [39, 46, 47] and microcavities [48] are capable of converting optical power in substrate and waveguide modes into out-coupled modes, resulting in substantially increased η_{out} . It was reported that a light-outcoupling hemispherical lens improved the peak EQEs of perovskite nanocrystal LEDs from 23.4% to 45.5% [49]. Microcavities were used to improve η_{out} from ~20% to ~30% for top-emitting PeLEDs featuring transparent electrodes, leading to peak EQEs of up to 20.2% [50]. Similarly, other light outcoupling approaches employing plasmonic effects [51, 52] and refractive index matching [53–55] were found to improve η_{out} for PeLEDs.

6 Challenges

While the researchers in the field have witnessed a remarkable progress in improving PeLED performance, many challenges remain. Some of the most critical current shortcomings of PeLEDs include poor operational stability, the low efficiencies of blue PeLEDs, the toxicity of lead, and the difficulty in micropatterning for mini/micro-PeLED applications.

6.1 Operational Stability

The poor operational stability of PeLEDs is the grandest challenge in their journey toward commercialization. Halide perovskite materials were widely considered to be intrinsically unstable under electric fields due to the ionic nature of their crystal lattices. Device lifetimes (T_{50}) are typically on the order of 10–100 hours. This is clearly unsatisfactory as practical applications require much improved device longevity (longer than 10,000 h at useful photon fluxes) [56].

A recent breakthrough in this area was the demonstration of efficient (peak EQE =22.8%) FAPbI₃ PeLEDs with ultralong operational lifetimes meeting the demands of commercial applications. This was enabled by the introduction of a dipolar molecular stabilizer, SFB10 [18]. The PeLEDs showed no degradation over 3600 h (5 months) under continuous operation at a current density of 5 mA cm⁻². Accelerated aging tests at current densities of 10–200 mA cm⁻² were performed to obtain the operational lifetimes of the PeLEDs, according to an empirical scaling law developed for modeling the degradation of LEDs:

$$R_0^n \times T_{50} = \text{constant} \quad (5)$$

where R_0 is the initial radiance of the LED and n is the acceleration factor. Based on the 62 data points acquired from the accelerated aging tests, T_{50} lifetimes were

estimated to be $\sim 1.2 \times 10^4$ h (~ 1.3 years) and $\sim 3.3 \times 10^4$ h (~ 3.7 years) at $3.7 \text{ W sr}^{-1} \text{ m}^{-2}$ (5 mA cm^{-2}) and $2.1 \text{ W sr}^{-1} \text{ m}^{-2}$ (3.2 mA cm^{-2}), respectively (Fig. 5a). Longer T_{50} lifetimes were estimated for lower radiances, for example, at $0.21 \text{ W sr}^{-1} \text{ m}^{-2}$ (0.7 mA cm^{-2}), the T_{50} lifetime was estimated to be 2.4×10^6 h (2.7 centuries). For reference, for high-efficiency OLEDs based on $\text{Ir}(\text{ppy})_3$, a luminance of 1000 cd m^{-2} corresponds to a radiance of $2.1 \text{ W sr}^{-1} \text{ m}^{-2}$, and a luminance of 100 cd m^{-2} corresponds to a radiance of $0.21 \text{ W sr}^{-1} \text{ m}^{-2}$. The dipolar molecular stabilizer interacts with the cations (FA^+ , Pb^{2+}) and anions (I^-) at the grain boundaries of the FAPbI_3 perovskite. This suppresses ion migration under electric fields, preventing the formation of lead iodide which mediates detrimental phase transformation. The ultralong device lifetimes could remove the critical concern that halide perovskite devices may be intrinsically unstable, paving the path toward industrial applications [18]. Despite these encouraging results, stable PeLEDs emitting in the visible spectral range are yet to be demonstrated.

Ion migration is a key mechanism limiting the operational stability of PeLEDs [59–61]. Owing to the soft and ionic crystal structure of the halide perovskites, ion migration may be triggered by external stimuli such as electric fields, heat, and light (Fig. 5b) [57, 59, 62]. Ionic movements would induce detrimental effects on the performance of PeLEDs through defect generation, lattice deformation, interfacial ion accumulation, ionic doping, and chemical interactions [59]. Apart from the aforementioned dipolar molecular stabilizer approach [18], a range of methods such as molecular passivation [2, 4, 63–68], dimensionality control [12, 69–71], and thermal management [72] were explored to suppress the effects of ion migration.

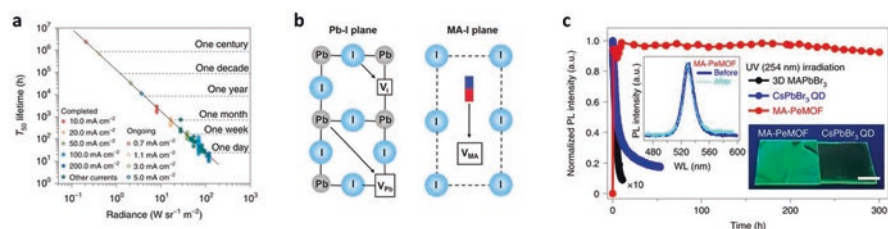


Fig. 5 Recent studies on PeLED operational stability and ion migration. (a) The T_{50} lifetimes as a function of initial radiance (R_0); the solid line is the fitting of the T_{50} data to equation $R_0^n \times T_{50} = \text{constant}$, where n is the acceleration factor ($n = 1.86$). The data points marked by the solid dots are from completed T_{50} measurements (total data points, 62). The open circles are the extrapolated T_{50} lifetimes for the ongoing measurements at medium and low current densities, which are expected to finish after longer times. (b) Ionic transport mechanisms in a $\text{CH}_3\text{NH}_3\text{PbI}_3$ perovskite structure. Schematic illustration of the three ionic transport mechanisms involving conventional vacancy hopping between neighboring positions: I^- migration along an octahedron edge; Pb^{2+} migration along the diagonal direction $\langle 110 \rangle$; CH_3NH_3^+ migration into a neighboring vacant A-site cage involving motion normal to the unit cell face composed of four iodide ions. (c) Normalized PL intensity as a function of time for 3D MAPbBr_3 , CsPbBr_3 QD, and MA-PeMOF thin films in ambient air (relative humidity of 30%) under constant UV irradiation (254 nm). Insets show the PL spectrum of the MA-PeMOF thin film before and after irradiation for 200 hours (left) and their photographs under UV light (right). Scale bar, 1 cm. WL, wavelength. Panel a was reproduced from [18]. Panel b was reproduced from [57]. Panel c was reproduced from [58]

Metal-organic frameworks (MOF) were reported to enable enhanced operational stability of PeLEDs by preventing ion migration in the perovskite-MOF emissive films (Fig. 5c), achieving bright and stable ($T_{50} > 50$ h) green EL [58]. A cross-linking strategy using methylene-bis-acrylamide was reported to strengthen the binding of Br^- and increase the activation energy of ion migration in bromide perovskite-based LEDs, leading to a T_{50} lifetime of 208 h [63]. As halide ions are widely considered to be the primary contributor to ion migration [60, 61], further efforts in the control of halide ions are expected to show benefits in improving device stability. This could be achieved in a number of ways, including raising the barriers to ion migration using molecular stabilizers [18] and reducing halide vacancies [73].

Phase transformation and halide segregation are some of the main factors for the instability of blue and red PeLEDs based on mixed-halide [74] and mixed-dimensional perovskites [71] and perovskite structures with undesirable tolerance factors [67, 75]. Common triggers for these processes include unfavorable material composition [71], halide migration [74], lattice strain/stress, and externally induced structural evolution [67, 75]. It is possible to partially suppress halide segregation by modifying the nanocrystal surfaces with multidentate ligands, hindering the formation of iodine Frenkel defects [68]. Despite such improvements, the T_{50} lifetime at an initial luminance of 141 cd m^{-2} was only 30 min for these devices, indicating that considerable challenges remain for mixed-halide PeLEDs [68]. Interfacial chemical interactions [65, 75] and thermal degradation [65] are some of the additional contributors to the structural instability of halide perovskites.

6.2 Blue PeLEDs

Unlike near-infrared, red and green PeLEDs exhibiting high EQEs of over 20%, the efficiencies of blue PeLEDs are still low. For “standard” blue PeLEDs with peak wavelengths equal to or shorter than 470 nm, the EQEs are below 10%, limiting their potential application in wide-color-gamut displays. Moreover, the operational stability of blue PeLEDs is significantly worse compared to PeLEDs emitting at longer wavelengths.

The most widely used method for achieving blue PeLEDs is the mixing of bromide- and chloride-based perovskite precursors (i.e., halide mixing). However, the PLQEs of the blue perovskite emitters normally reduce as the chloride fraction increases, owing to the small formation energy of chloride vacancies [73]. Blue-emitting perovskites prepared from bromide-chloride mixing often show undesirable Goldschmidt tolerance factors, resulting in reduced stability [76]. Besides, the halide vacancies are active sites for ion migration, leading to spectral and structural instability [67, 75].

An alternative approach for attaining blue PeLEDs is through quantum confinement effects in reduced-dimensional bromide perovskites, shifting the emission

wavelengths from the green to blue regions. These typically include quasi-2D/3D perovskites [77] and perovskite nanocrystals/quantum dots [19]. Reduced-dimensional perovskites show advantages in PLQEs due to the generally larger exciton binding energies [28, 78] or fast-energy transfer/funneling processes [11, 12] that increase the probability of electron-hole encounters, and the improved passivation [3] of nanocrystalline perovskite grains. For quasi-2D/3D perovskite systems, a main challenge lies in the difficulty in attaining uniform phase distribution for blue EL with high spectral purity [77]. Similarly, for perovskite nanocrystals (including quantum dots), the broad distribution of nanocrystal sizes could result in a wider emission bandwidth due to the bandgap variations of the nanocrystals, affecting the spectral narrowness of EL.

While a few recent works reported efficient blue PeLEDs with EQEs > 10% [20, 79, 80], the EL emission was still limited to the sky-blue spectral region (475–495 nm), deviating from the requirements of high-definition displays. Understanding the nucleation and crystallization processes and the origin of nonradiative losses in blue perovskite emitters may lead to further advances in this area. Achieving stable operation with blue PeLEDs presents even greater challenges and is expected to be a subject of future research.

6.3 Toxicity

Similar to perovskite solar cells, high-performance PeLEDs are typically based on lead halide perovskites. The potential toxicity of metallic lead (Pb) in the perovskite materials raises concerns over the possible impacts to human health and the natural environment, limiting the scope of practical applications. The search for eco-friendly alternatives to the lead-based perovskites is therefore an important direction in the area of PeLEDs.

Some of the most widely used methods for the reduction of toxicity include partial or complete replacement of Pb with other group-IV metals (e.g., Sn [81–83] and Ge [23]) and double perovskites [21]. As Pb-based perovskites generally show superior optoelectronic properties, replacing Pb with nontoxic elements while maintaining high device performance is a clear goal in this direction.

Replacing Pb with Sn was found to be effective in producing efficient perovskite solar cells with reduced toxicity. However, Sn-based (including Pb-Sn) perovskites generally show significantly reduced PLQEs compared to the Sn-free, Pb-based perovskites. This might be due to the reason that it is more likely to form a higher density of trap states related to the oxidation of Sn²⁺ and the rapid crystallization of Sn-based perovskites [81]. Decent EQEs of up to ~5% from Sn-based perovskite LEDs were reported [82, 83], but the overall device performance remained unsatisfactory.

Recently, it was shown that it is possible to prepare highly luminescent Ge-Pb perovskite films with PLQEs of up to ~71%. This led to the demonstration of

efficient green PeLEDs with EQEs of up to 13.1% [23]. While this indicates new opportunities in this direction, achieving high efficiencies for lead-free PeLEDs remains to be a challenging task.

Double perovskites, with a general formula of $A_2B^I B^{III} X_6$, is another important material class for lead-free devices [21]. While a wide variety of material compositions can be expected from this class of perovskites, currently they exhibit low PLQEs [84], largely due to the indirect bandgap nature and the high densities of traps for most of the double perovskites developed. Metal ion dopants were used to raise the PLQEs of double perovskites. For instance, by introducing Bi^{3+} and Na^+ , $Cs_2Ag_{0.6}Na_{0.4}InCl_6:0.04\%$ Bi powders showed a PLQE of $\sim 86\%$, three orders of magnitude higher than that of $Cs_2AgInCl_6$ [21]. However, preparing efficient PeLEDs based on double perovskites remains very challenging, partly owing to the limited quality of the perovskite films [21].

6.4 Mini- and Micro-PeLEDs

Mini- and micro-light-emitting diodes (mini/micro-LEDs) [85–88] have attracted much attention owing to their superior characteristics of low power consumption, high contrast ratio, high brightness, high response speed, and high efficiency. While the current mini/micro-LED technologies are known to be advantageous, the requirement for high-quality epitaxial III-V semiconductors becomes more stringent, as reducing the pixel sizes to the microscopic scale tends to generate nonradiative loss pathways near the sidewalls of the active regions [86, 89]. Besides, the mass-transfer process required for the production of mini/micro-LED displays reduces the manufacturing yields [90–92]. These factors inevitably increase the production costs of mini/micro-LEDs.

Despite the promise of PeLEDs as a low-cost alternative to the mainstream LED technologies, the options for creating efficient PeLEDs with microscopic pixel sizes remain limited, leading to moderate emission efficiencies from PeLEDs with micropatterned emissive arrays [93, 94]. The possibility of developing single-pixel mini/micro-PeLEDs is rarely explored.

Recently, efficient mini/micro-perovskite LEDs were reported. The compatibility of luminescent perovskite with self-aligned photolithography (Fig. 6) was enabled by the insertion of a lithium fluoride surface-tension-relief layer. Active-layer luminescence properties and morphological control are critical to mini/micro-PeLEDs. Following these design rules, proof-of-concept mini/micro-PeLEDs with active pixel areas of down to $100 \times 200 \text{ um}^2$, and peak external quantum efficiencies of up to $\sim 9.1\%$, were developed [25]. While this study indicated the potential of next-generation mini/micro-PeLED displays, such applications demand individually addressable pixel arrays with considerably smaller pixel sizes comparable to commercial micro-LEDs.

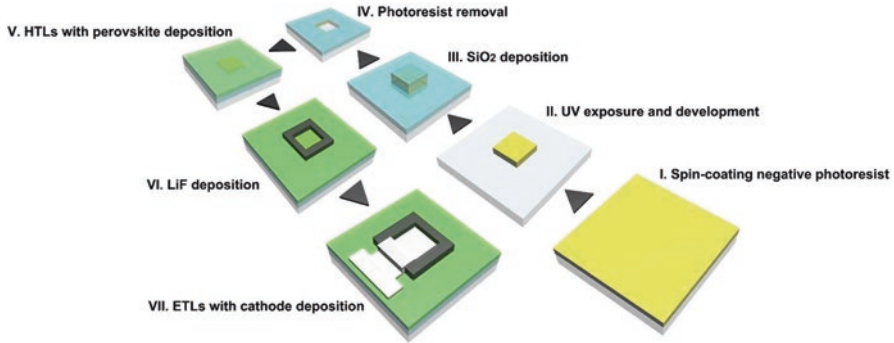


Fig. 6 Illustration of self-aligned micropatterning processes for mini/micro-PeLEDs. (I) Spin-coating negative photoresist. (II) UV exposure and development. (III) SiO₂ deposition. (IV) Photoresist removal. (V) HTLs with perovskite deposition. (VI) LiF deposition. (VII) ETLs with cathode deposition. Figure 6 was reproduced from [25]

7 Summary

PeLEDs have been recognized as an emerging technology for display, lighting, and communication applications. In this chapter, we have provided an overview of the basic designs, operating principles, and main challenges of PeLEDs. While the device architectures and fabrication processes of PeLEDs are similar to that of perovskite solar cells and solution-processed OLEDs, they exhibit some interesting light emission characteristics comparable to LEDs based on III-V semiconductors [9, 10]. The excellent spectral tunability and narrow emission linewidth of PeLEDs are potentially advantageous over that of OLEDs. The rapid progress in device efficiencies was primarily driven by material design and device engineering, leading to IQEs of approaching 100%. The suppression of both bulk and interfacial nonradiative recombination losses was key to reaching this goal. Opportunities in raising the EQEs of PeLEDs beyond the current state-of-the-art (20–28%) [2–6, 15] lie in the improvement of light outcoupling from the devices.

Looking forward, many challenges remain in developing PeLEDs from a laboratory curiosity to a commercially viable technology. A recent breakthrough was made in addressing the critical challenge of device instability [18], demonstrating NIR PeLEDs with ultralong operational lifetimes meeting the demands of practical applications. However, similar device stability is yet to be achieved for PeLEDs emitting in the visible region. Moreover, blue and low-toxicity PeLEDs face considerable challenges in raising the efficiency and stability beyond what can be currently achieved. While technical difficulties are present in the reliable micropatterning of perovskite devices, mini/micro-PeLEDs [25] are a promising research direction toward high-pixel-density display applications. Despite the challenges ahead, PeLEDs have set the sail for becoming a next-generation light source technology.

References

1. Tan, Z.-K., Moghaddam, R. S., Lai, M. L., Docampo, P., Higler, R., Deschler, F., Price, M., Sadhanala, A., Pazos, L. M., Credgington, D., Hanusch, F., Bein, T., Snaith, H. J., & Friend, R. H. (2014). *Nature Nanotechnology*, 9, 687.
2. Cao, Y., Wang, N., Tian, H., Guo, J., Wei, Y., Chen, H., Miao, Y., Zou, W., Pan, K., He, Y., Cao, H., Ke, Y., Xu, M., Wang, Y., Yang, M., Du, K., Fu, Z., Kong, D., Dai, D., Jin, Y., Li, G., Li, H., Peng, Q., Wang, J., & Huang, W. (2018). *Nature*, 562, 249.
3. Zhao, B., Bai, S., Kim, V., Lamboll, R., Shivanna, R., Auras, F., Richter, J. M., Yang, L., Dai, L., Alsari, M., She, X.-J., Liang, L., Zhang, J., Lilliu, S., Gao, P., Snaith, H. J., Wang, J., Greenham, N. C., Friend, R. H., & Di, D. (2018). *Nature Photonics*, 12, 783.
4. Lin, K., Xing, J., Quan, L. N., de Arquer, F. P. G., Gong, X., Lu, J., Xie, L., Zhao, W., Zhang, D., Yan, C., Li, W., Liu, X., Lu, Y., Kirman, J., Sargent, E. H., Xiong, Q., & Wei, Z. (2018). *Nature*, 562, 245.
5. Chiba, T., Hayashi, Y., Ebe, H., Hoshi, K., Sato, J., Sato, S., Pu, Y.-J., Ohisa, S., & Kido, J. (2018). *Nature Photonics*, 12, 681.
6. Liu, Z., Qiu, W., Peng, X., Sun, G., Liu, X., Liu, D., Li, Z., He, F., Shen, C., Gu, Q., Ma, F., Yip, H. L., Hou, L., Qi, Z., & Su, S. J. (2021). *Advanced Materials*, 33, 2103268.
7. Lee, M. M., Teuscher, J., Miyasaka, T., Murakami, T. N., & Snaith, H. J. (2012). *Science*, 338, 643.
8. Burroughes, J. H. H., Bradley, D. D. C., Brown, A. R., Marks, R. N., Mackay, K., Friend, R. H., Burns, P. L., Holmes, A. B., & Road, M. (1990). *Nature*, 347, 539.
9. Stranks, S. D., & Snaith, H. J. (2015). *Nature Nanotechnology*, 10, 391.
10. Liu, X. K., Xu, W., Bai, S., Jin, Y., Wang, J., Friend, R. H., & Gao, F. (2020). *Nature Materials*, 20(1), 10.
11. Yuan, M., Quan, L. N., Comin, R., Walters, G., Sabatini, R., Voznyy, O., Hoogland, S., Zhao, Y., Beauregard, E. M., Kanjanaboos, P., Lu, Z., Kim, D. H., & Sargent, E. H. (2016). *Nature Nanotechnology*, 11, 872.
12. Wang, N., Cheng, L., Ge, R., Zhang, S., Miao, Y., Zou, W., Yi, C., Sun, Y., Cao, Y., Yang, R., Wei, Y., Guo, Q., Ke, Y., Yu, M., Jin, Y., Liu, Y., Ding, Q., Di, D., Yang, L., Xing, G., Tian, H., Jin, C., Gao, F., Friend, R. H., Wang, J., & Huang, W. (2016). *Nature Photonics*, 10, 699.
13. Zhao, B., Lian, Y., Cui, L., Divitini, G., Kusch, G., Ruggeri, E., Auras, F., Li, W., Yang, D., Zhu, B., Oliver, R. A., MacManus-Driscoll, J. L., Stranks, S. D., Di, D., & Friend, R. H. (2020). *Nature Electronics*, 3, 704.
14. Cho, H., Jeong, S.-H., Park, M.-H., Kim, Y.-H., Wolf, C., Lee, C.-L., Heo, J. H., Sadhanala, A., Myoung, N., Yoo, S., Im, S. H., Friend, R. H., & Lee, T.-W. (2015). *Science*, 350, 1222.
15. Xu, W., Hu, Q., Bai, S., Bao, C., Miao, Y., Yuan, Z., Borzda, T., Barker, A. J., Tyukalova, E., Hu, Z., Kawecki, M., Wang, H., Yan, Z., Liu, X., Shi, X., Uvdal, K., Fahlman, M., Zhang, W., Duchamp, M., Liu, J.-M., Petrozza, A., Wang, J., Liu, L.-M., Huang, W., & Gao, F. (2019). *Nature Photonics*, 13, 418.
16. Cho, C., Zhao, B., Tainter, G. D., Lee, J. Y., Friend, R. H., Di, D., Deschler, F., & Greenham, N. C. (2020). *Nature Communications*, 11, 611.
17. Shi, X. B., Liu, Y., Yuan, Z., Liu, X. K., Miao, Y., Wang, J., Lenk, S., Reineke, S., & Gao, F. (2018). *Advanced Optical Materials*, 6, 1800667.
18. Guo, B., Lai, R., Jiang, S., Zhou, L., Ren, Z., Lian, Y., Li, P., Cao, X., Xing, S., Wang, Y., Li, W., Zou, C., Chen, M., Hong, Z., Li, C., Zhao, B., & Di, D. (2022). *Nature Photonics*, 16(9), 637.
19. Liu, Y., Cui, J., Du, K., Tian, H., He, Z., Zhou, Q., Yang, Z., Deng, Y., Chen, D., Zuo, X., Ren, Y., Wang, L., Zhu, H., Zhao, B., Di, D., Wang, J., Friend, R. H., & Jin, Y. (2019). *Nature Photonics*, 13, 760.
20. Karlsson, M., Yi, Z., Reichert, S., Luo, X., Lin, W., Zhang, Z., Bao, C., Zhang, R., Bai, S., Zheng, G., Teng, P., Duan, L., Lu, Y., Zheng, K., Pullerits, T., Deibel, C., Xu, W., Friend, R., & Gao, F. (2021). *Nature Communications*, 12, 1.

21. Luo, J., Wang, X., Li, S., Liu, J., Guo, Y., Niu, G., Yao, L., Fu, Y., Gao, L., Dong, Q., Zhao, C., Leng, M., Ma, F., Liang, W., Wang, L., Jin, S., Han, J., Zhang, L., Etheridge, J., Wang, J., Yan, Y., Sargent, E. H., & Tang, J. (2018). *Nature*, 563, 541.
22. Chen, J., Wang, J., Xu, X., Li, J., Song, J., Lan, S., Liu, S., Cai, B., Han, B., Precht, J. T., Ginger, D., & Zeng, H. (2020). *Nature Photonics*, 15, 238.
23. Yang, D., Zhang, G., Lai, R., Cheng, Y., Lian, Y., Rao, M., Huo, D., Lan, D., Zhao, B., & Di, D. (2021). *Nature Communications*, 12, 4295.
24. Lu, J., Guan, X., Li, Y., Lin, K., Feng, W., Zhao, Y., Yan, C., Li, M., Shen, Y., Qin, X., & Wei, Z. (2021). *Advanced Materials*, 33, 2104414.
25. Hsu, C., Tian, S., Lian, Y., Zhang, G., Zhou, Q., Cao, X., Zhao, B., & Di, D. (2021). *Cell Reports Physical Science*, 2, 100582.
26. Lian, Y., Lan, D., Xing, S., Guo, B., Ren, Z., Lai, R., Zou, C., Zhao, B., Friend, R. H., & Di, D. (2022). *Nature Communications*, 13, 3845.
27. Wang, J., Wang, N., Jin, Y., Si, J., Tan, Z.-K. K., Du, H., Cheng, L., Dai, X., Bai, S., He, H., Ye, Z., Lai, M. L., Friend, R. H., & Huang, W. (2015). *Advanced Materials*, 27, n/a.
28. Stranks, S. D., Hoyer, R. L. Z., Di, D., Friend, R. H., Deschler, F., Stranks, S. D., Hoyer, R. L. Z., Di, D., Friend, R. H., & Deschler, F. (2019). *Advanced Materials*, 31, 1803336.
29. Richter, J. M., Abdi-Jalebi, M., Sadhanala, A., Tabachnyk, M., Rivett, J. P. H., Pazos-Outón, L. M., Gödel, K. C., Price, M., Deschler, F., & Friend, R. H. (2016). *Nature Communications*, 7, 13941.
30. Landsberg, P. T. (1992). *Recombination in semiconductors*. Cambridge University Press. <https://doi.org/10.1017/CBO9780511470769>
31. Di, D., Yang, L., Richter, J. M., Meraldi, L., Altamimi, R. M., Alyamani, A. Y., Credgington, D., Musselman, K. P., MacManus-Driscoll, J. L., & Friend, R. H. (2017). *Advanced Materials*, 29, 1605987.
32. Di, D., Romanov, A. S., Yang, L., Richter, J. M., Rivett, J. P. H., Jones, S., Thomas, T. H., Abdi Jalebi, M., Friend, R. H., Linnolahti, M., Bochmann, M., & Credgington, D. (2017). *Science*, 356, 159.
33. Jiang, Y., Cui, M., Li, S., Sun, C., Huang, Y., Wei, J., Zhang, L., Lv, M., Qin, C., Liu, Y., & Yuan, M. (2021). *Nature Communications*, 12, 1.
34. Zhao, X., & Tan, Z. K. (2019). *Nature Photonics*, 14(4), 215.
35. Xiao, Z., Kerner, R. A., Zhao, L., Tran, N. L., Lee, K. M., Koh, T.-W., Scholes, G. D., & Rand, B. P. (2017). *Nature Photonics*, 11, 108.
36. Ban, M., Zou, Y., Rivett, J. P. H., Yang, Y., Thomas, T. H., Tan, Y., Song, T., Gao, X., Credgington, D., Deschler, F., Sirringhaus, H., & Sun, B. (2018). *Nature Communications*, 9, 3892.
37. Choul Yu, J., Kim, D. B., Baek, G., Lee, B. R., Jung, E. D., Lee, S., Chu, J. H., Lee, D.-K., Choi, K. J., Cho, S., Song, M. H., Yu, J. C., Kim, D. B., Lee, B. R., Jung, E. D., Lee, S., Choi, K. J., Song, M. H., Baek, G., Cho, S., Chu, J. H., & Lee, D. (2015). *Advanced Materials*, 27, 3492.
38. Li, G., Rivarola, F. W. R., Davis, N. J. L. K., Bai, S., Jellicoe, T. C., de la Peña, F., Hou, S., Ducati, C., Gao, F., Friend, R. H., Greenham, N. C., & Tan, Z.-K. (2016). *Advanced Materials*, 28, 3528.
39. Shen, Y., Cheng, L.-P., Li, Y.-Q., Li, W., Chen, J.-D., Lee, S.-T., Tang, J.-X., Shen, Y., Cheng, L.-P., Li, Y.-Q., Li, W., Chen, J.-D., Lee, S.-T., & Tang, J.-X. (2019). *Advanced Materials*, 31, 1901517.
40. Fieramosca, A., de Marco, L., Passoni, M., Polimeno, L., Rizzo, A., Rosa, B. L. T., Cruciani, G., Dominici, L., de Giorgi, M., Gigli, G., Andreani, L. C., Gerace, D., Ballarini, D., & Sanvitto, D. (2018). *ACS Photonics*, 5, 4179.
41. Walters, G., Haeberlé, L., Quintero-Bermudez, R., Brodeur, J., Kéna-Cohen, S., & Sargent, E. H. (2020). *Journal of Physical Chemistry Letters*, 11, 3458.
42. Jurow, M. J., Lampe, T., Penzo, E., Kang, J., Koc, M. A., Zechel, T., Nett, Z., Brady, M., Wang, L. W., Alivisatos, A. P., Cabrini, S., Brütting, W., & Liu, Y. (2017). *Nano Letters*, 17, 4534.
43. Zou, C., & Lin, L. Y. (2020). *Optics Letters*, 45(17), 4786–4789.

44. Jurow, M. J., Morgenstern, T., Eisler, C., Kang, J., Penzo, E., Do, M., Engelmayer, M., Osowiecki, W. T., Bekenstein, Y., Tassone, C., Wang, L. W., Alivisatos, A. P., Brütting, W., & Liu, Y. (2019). *Nano Letters*, 19, 2489.
45. Bowman, A. R., Anaya, M., Greenham, N. C., & Stranks, S. D. (2020). *Physical Review Letters*, 125, 067401.
46. Kim, H. P., Kim, J., Kim, B. S., Kim, H. M., Kim, J., Bin, A. R., Yusoff, M., Jang, J., & Nazeeruddin, M. K. (2017). *Advanced Optical Materials*, 5, 1600920.
47. Möller, S., & Forrest, S. R. (2002). *Journal of Applied Physics*, 91, 3324.
48. Schubert, E. F., Hunt, N. E. J., Micovic, M., Malik, R. J., Sivco, D. L., Cho, A. Y., & Zydzik, G. J. (1994). *Science* (1979), 265, 943.
49. Kim, Y. H., Kim, S., Kakekhani, A., Park, J., Park, J., Lee, Y. H., Xu, H., Nagane, S., Wexler, R. B., Kim, D. H., Jo, S. H., Martínez-Sarti, L., Tan, P., Sadhanala, A., Park, G. S., Kim, Y. W., Hu, B., Bolink, H. J., Yoo, S., Friend, R. H., Rappe, A. M., & Lee, T. W. (2021). *Nature Photonics*, 15(2), 148.
50. Miao, Y., Cheng, L., Zou, W., Gu, L., Zhang, J., Guo, Q., Peng, Q., Xu, M., He, Y., Zhang, S., Cao, Y., Li, R., Wang, N., Huang, W., & Wang, J. (2020). *Light: Science & Applications*, 9, 1.
51. Zhang, X., Xu, B., Wang, W., Liu, S., Zheng, Y., Chen, S., Wang, K., & Sun, X. W. (2017). *ACS Applied Materials & Interfaces*, 9, 4926.
52. Luo, Q., Zhang, C., Deng, X., Zhu, H., Li, Z., Wang, Z., Chen, X., & Huang, S. (2017). *ACS Applied Materials & Interfaces*, 9, 34821.
53. Berestennikov, A. S., Voroshilov, P. M., Makarov, S. V., & Kivshar, Y. S. (2019). *Applied Physics Reviews*, 6, 031307.
54. Lova, P., Cortecchia, D., Krishnamoorthy, H. N. S., Giusto, P., Bastianini, C., Bruno, A., Comoretto, D., & Soci, C. (2018). *ACS Photonics*, 5, 867.
55. Chen, S., & Nurmikko, A. (2017). *ACS Photonics*, 4, 2486.
56. Wellmann, P., Hofmann, M., Zeika, O., Werner, A., Birnstock, J., Meerheim, R., He, G., Walzer, K., Pfeiffer, M., & Leo, K. (2005). *Journal of the Society for Information Display*, 13, 393.
57. Eames, C., Frost, J. M., Barnes, P. R. F., O'Regan, B. C., Walsh, A., & Islam, M. S. (2015). *Nature Communications*, 6, 1.
58. Tsai, H., Shrestha, S., Vilá, R. A., Huang, W., Liu, C., Hou, C. H., Huang, H. H., Wen, X., Li, M., Wiederrecht, G., Cui, Y., Cotlet, M., Zhang, X., Ma, X., & Nie, W. (2021). *Nature Photonics*, 15, 843.
59. Dong, Q., Lei, L., Mendes, J., & So, F. (2020). *Journal of Physics: Materials*, 3, 012002.
60. Li, C., Wang, N., Guerrero, A., Zhong, Y., Long, H., Miao, Y., Bisquert, J., Wang, J., & Huettnner, S. (2019). *Journal of Physical Chemistry Letters*, 10, 6857.
61. Li, C., Guerrero, A., Huettnner, S., & Bisquert, J. (2018). *Nature Communications*, 9, 5113.
62. Boyd, C. C., Checharoen, R., Leijtens, T., & McGehee, M. D. (2019). *Chemical Reviews*, 119, 3418.
63. Han, B., Yuan, S., Cai, B., Song, J., Liu, W., Zhang, F., Fang, T., Wei, C., Zeng, H., Han, B., Yuan, S., Cai, B., Song, J., Liu, W., Zhang, F., Fang, T., Wei, C., & Zeng, H. (2021). *Advanced Functional Materials*, 31, 2011003.
64. Li, H., Lin, H., Ouyang, D., Yao, C., Li, C., Sun, J., Song, Y., Wang, Y., Yan, Y., Wang, Y., Dong, Q., & Choy, W. C. H. (2021). *Advanced Materials*, 33, 2008820.
65. Kuang, C., Hu, Z., Yuan, Z., Wen, K., Qing, J., Kobera, L., Abbrent, S., Brus, J., Yin, C., Wang, H., Xu, W., Wang, J., Bai, S., & Gao, F. (2021). *Joule*, 5, 618.
66. Wang, H., Zhang, X., Wu, Q., Cao, F., Yang, D., Shang, Y., Ning, Z., Zhang, W., Zheng, W., Yan, Y., Kershaw, S. V., Zhang, L., Rogach, A. L., & Yang, X. (2019). *Nature Communications*, 10, 1.
67. Jeong, B., Han, H., Ji Choi, Y., Hwan Cho, S., Hyuk Kim, E., Won Lee, S., Sung Kim, J., Park, C., Kim, D., Park, C., Jeong, B., Han, H., Cho, S. H., Kim, E. H., Lee, S. W., Kim, J. S., Park, C., Choi, Y. J., & Kim, D. (2018). *Advanced Functional Materials*, 28, 1706401.
68. Hassan, Y., Park, J. H., Crawford, M. L., Sadhanala, A., Lee, J., Sadighian, J. C., Mosconi, E., Shivanna, R., Radicchi, E., Jeong, M., Yang, C., Choi, H., Park, S. H., Song, M. H., de Angelis, F., Wong, C. Y., Friend, R. H., Lee, B. R., & Snaith, H. J. (2021). *Nature*, 591, 7848.

69. Ma, D., Lin, K., Dong, Y., Choubisa, H., Proppe, A. H., Wu, D., Wang, Y. K., Chen, B., Li, P., Fan, J. Z., Yuan, F., Johnston, A., Liu, Y., Kang, Y., Lu, Z. H., Wei, Z., & Sargent, E. H. (2021). *Nature*, 599, 7886.
70. Wang, Q., Wang, X., Yang, Z., Zhou, N., Deng, Y., Zhao, J., Xiao, X., Rudd, P., Moran, A., Yan, Y., & Huang, J. (2019). *Nature Communications*, 10, 1.
71. Xing, J., Zhao, Y., Askerka, M., Quan, L. N., Gong, X., Zhao, W., Zhao, J., Tan, H., Long, G., Gao, L., Yang, Z., Voznyy, O., Tang, J., Lu, Z. H., Xiong, Q., & Sargent, E. H. (2018). *Nature Communications*, 9, 1.
72. Zhao, L., Roh, K., Kacmoli, S., Al Kurdi, K., Jhulki, S., Barlow, S., Marder, S. R., Gmachl, C., & Rand, B. P. (2020). *Advanced Materials*, 32, 2000752.
73. Zheng, X., Yuan, S., Liu, J., Yin, J., Yuan, F., Shen, W. S., Yao, K., Wei, M., Zhou, C., Song, K., Zhang, B. B., Lin, Y., Hedhili, M. N., Wehbe, N., Han, Y., Sun, H. T., Lu, Z. H., Anthopoulos, T. D., Mohammed, O. F., Sargent, E. H., Liao, L. S., & Bakr, O. M. (2020). *ACS Energy Letters*, 5, 793.
74. Vashishtha, P., & Halpert, J. E. (2017). *Chemistry of Materials*, 29, 5965.
75. Yuan, Z., Miao, Y., Hu, Z., Xu, W., Kuang, C., Pan, K., Liu, P., Lai, J., Sun, B., Wang, J., Bai, S., & Gao, F. (2019). *Nature Communications*, 10, 1.
76. Yoon, S. J., Kuno, M., & Kamat, P. V. (2017). *ACS Energy Letters*, 2, 1507.
77. Yuan, S., Wang, Z.-K., Xiao, L.-X., Zhang, C.-F., Yang, S.-Y., Chen, B.-B., Ge, H.-T., Tian, Q.-S., Jin, Y., Liao, L.-S., Yuan, S., Wang, Z.-K., Yang, S.-Y., Ge, H.-T., Tian, Q.-S., Jin, Y., Liao, L.-S., Xiao, L.-X., Zhang, C.-F., & Chen, B.-B. (2019). *Advanced Materials*, 31, 1904319.
78. Congreve, D. N., Weidman, M. C., Seitz, M., Paritmongkol, W., Dahod, N. S., & Tisdale, W. A. (2017). *ACS Photonics*, 4, 476.
79. Yang, Y., Xu, S., Ni, Z., van Brackle, C. H., Zhao, L., Xiao, X., Dai, X., & Huang, J. (2021). *Advanced Materials*, 33, 2100783.
80. Liu, Y., Li, Z., Xu, J., Dong, Y., Chen, B., Park, S. M., Ma, D., Lee, S., Huang, J. E., Teale, S., Voznyy, O., & Sargent, E. H. (2022). *Journal of the American Chemical Society*, 144, 4009.
81. Jia, H., Shi, H., Yu, R., Ma, H., Wang, Z., Zou, C., Tan, Z. A., Jia, H., Shi, H., Yu, R., Ma, H., Tan, Z., Wang, Z., & Zou, C. (2022). *Small*, 18, 2200036.
82. Wang, Y., Zou, R., Chang, J., Fu, Z., Cao, Y., Zhang, L., Wei, Y., Kong, D., Zou, W., Wen, K., Fan, N., Wang, N., Huang, W., & Wang, J. (2019). *Journal of Physical Chemistry Letters*, 10, 453.
83. Lu, J., Guan, X., Li, Y., Lin, K., Feng, W., Zhao, Y., Yan, C., Li, M., Shen, Y., Qin, X., Wei, Z., Lu, J., Guan, X., Li, Y., Lin, K., Feng, W., Zhao, Y., Yan, C., Li, M., Shen, Y., Qin, X., & Wei, Z. (2021). *Advanced Materials*, 33, 2104414.
84. Wang, C. Y., Liang, P., Xie, R. J., Yao, Y., Liu, P., Yang, Y., Hu, J., Shao, L., Sun, X. W., Kang, F., & Wei, G. (2020). *Chemistry of Materials*, 32, 7814.
85. Jin, S. X., Li, J., Li, J. Z., Lin, J. Y., & Jiang, H. X. (2000). *Applied Physics Letters*, 76, 631.
86. Wong, M. S., Nakamura, S., & DenBaars, S. P. (2020). *ECS Journal of Solid State Science and Technology*, 9, 015012.
87. Lin, J. Y., & Jiang, H. X. (2020). *Applied Physics Letters*, 116, 100502.
88. Huang, Y., Hsiang, E. L., Deng, M. Y., & Wu, S. T. (2020). *Light: Science & Applications*, 9, 1.
89. Cao, X. A., Pearton, S. J., Zhang, A. P., Dang, G. T., Ren, F., Shul, R. J., Zhang, L., Hickman, R., & van Hove, J. M. (1999). *Applied Physics Letters*, 75, 2569.
90. Corbett, B., Loi, R., Zhou, W., Liu, D., & Ma, Z. (2017). *Progress in Quantum Electronics*, 52, 1.
91. Cok, R. S., Meitl, M., Rotzoll, R., Melnik, G., Fecioru, A., Trindade, A. J., Raymond, B., Bonafede, S., Gomez, D., Moore, T., Prevatte, C., Radauscher, E., Goodwin, S., Hines, P., & Bower, C. A. (2017). *Journal of the Society for Information Display*, 25, 589.
92. Zhang, L., Ou, F., Chong, W. C., Chen, Y., & Li, Q. (2018). *Journal of the Society for Information Display*, 26, 137.
93. Zou, C., Chang, C., Sun, D., Böhringer, K. F., & Lin, L. Y. (2020). *Nano Letters*, 20, 3710.
94. Zou, C., Liu, Y., Ginger, D. S., & Lin, L. Y. (2020). *ACS Nano*, 14, 6076.